Article

Cell Reports

The P72R Polymorphism of p53 Predisposes to Obesity and Metabolic Dysfunction

Graphical Abstract

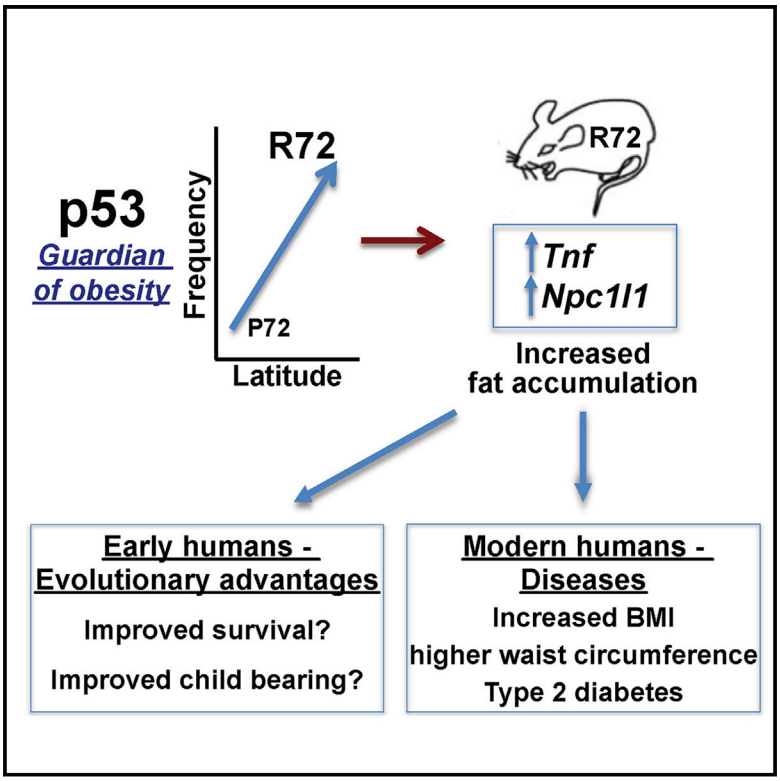

Highlights

- A high-fat diet was fed to mice containing P72 and R72 variants of p53
- Significantly increased fat accumulation was evident in R72 mice
- Significant increases in two p53 target genes, *Tnf* and *Npc1l1*, occurred in R72 mice
- Inhibitors of Tnf and Npc1l1 block the increased weight gain in R72 mice

Authors

Che-Pei Kung, Julia I-Ju Leu, Subhasree Basu, ..., Donna L. George, Rexford S. Ahima, Maureen E. Murphy

Correspondence

mmurphy@wistar.org

In Brief

Kung et al. show that the R72 variant of p53 leads to increased obesity and glucose intolerance in mice fed a high-fat diet. They identify two p53 target genes, Tnf and Npc1l1, that are preferentially bound by R72 and that are responsible for this phenotype.

Kung et al., 2016, Cell Reports *14*, 2413–2425
March 15, 2016
http://dx.doi.org/10.1016/j.celrep.2016.02.037

CellPress

Cell Reports
Article

The P72R Polymorphism of p53 Predisposes to Obesity and Metabolic Dysfunction

Che-Pei Kung,[1] Julia I-Ju Leu,[2] Subhasree Basu,[1] Sakina Khaku,[1] Frederick Anokye-Danso,[3] Qin Liu,[1,4] Donna L. George,[2] Rexford S. Ahima,[3] and Maureen E. Murphy[1,*]
[1]Molecular and Cellular Oncogenesis Program, The Wistar Institute, Philadelphia, PA 19104, USA
[2]Department of Genetics
[3]Institute for Diabetes, Obesity, and Metabolism
The Perelman School at the University of Pennsylvania School of Medicine, Philadelphia, PA 19104, USA
[4]Biostatistics Unit, The Wistar Institute, Philadelphia, PA 19104, USA
*Correspondence: mmurphy@wistar.org
http://dx.doi.org/10.1016/j.celrep.2016.02.037

SUMMARY

p53 is well known for its tumor suppressor role, but this protein also has a poorly understood role in the regulation of metabolism. Human studies have implicated a common polymorphism at codon 72 of p53 in diabetic and pre-diabetic phenotypes. To understand this role, we utilized a humanized mouse model of the p53 codon 72 variants and monitored these mice following challenge with a high-fat diet (HFD). Mice with the arginine 72 (R72) variant of p53 developed more-severe obesity and glucose intolerance on a HFD, compared to mice with the proline 72 variant (P72). R72 mice developed insulin resistance, islet hypertrophy, increased infiltration of immune cells, and fatty liver disease. Gene expression analyses and studies with small-molecule inhibitors indicate that the p53 target genes *Tnf* and *Npc1l1* underlie this phenotype. These results shed light on the role of p53 in obesity, metabolism, and inflammation.

INTRODUCTION

The p53 tumor suppressor protein has a well-established role in the suppression of cancer (Levine and Oren, 2009). This protein confers its tumor-suppressive activities predominantly by acting as a transcription factor, transactivating over 200 different target genes. p53 has also been found to be a critical factor governing innate and adaptive immune responses, reproduction, development, neural degeneration, and aging (Chang et al., 2012; Danilova et al., 2008; Levine et al., 2011; Menendez et al., 2013; Poyurovsky and Prives, 2010). More recently, the relationship between p53 and metabolism has become the focus of new studies, particularly with the revelation that the role of p53 in metabolism may be essential to its tumor suppressor function (Li et al., 2012; Long et al., 2013; Maddocks et al., 2013; Vousden and Ryan, 2009). Additionally, considerable evidence points to a crucial role for p53 in metabolic diseases such as cardiovascular disease, obesity, and type 2 diabetes (Minamino et al., 2009; Ortega et al., 2014; Sano et al., 2007; Tavana et al., 2010).

Genetic polymorphisms arise over time and are largely responsible for population diversity. Though largely considered innocuous, some SNPs can have significant biological consequences (Chen and Shen, 2015; De Iuliis et al., 2015). The most-common p53 SNP occurs at amino acid codon 72, where the nucleotide sequence CCC or CGC encodes proline (P72) or arginine (R72) at this residue, respectively (rs1042522; P72R). Interestingly, the frequency of the R72 variant is associated with increasing latitude and colder winter temperatures (Beckman et al., 1994; Shi et al., 2009). A number of studies indicate that the codon 72 polymorphism of p53 alters its function. In response to DNA damage, the P72 variant promotes enhanced cell-cycle arrest (Pim and Banks, 2004; Thomas et al., 1999), whereas the R72 variant is a superior inducer of apoptosis (Azzam et al., 2013; Bergamaschi et al., 2006; Dumont et al., 2003; Kung et al., 2015). These studies prompted a number of efforts to correlate the codon 72 polymorphism with cancer risk, but the contribution of this polymorphism to cancer risk is only weakly supported (Whibley et al., 2009), and genome-wide association studies (GWASs) on the codon 72 SNP of p53 have failed to reveal significant associations of this SNP with cancer risk (http://www.gwascentral.org).

In contrast to the lack of cancer associations, GWAS analyses have uncovered significant associations between the R72 variant and increased BMI (Speliotes et al., 2010). In addition, large-scale candidate gene analyses have pointed to a role for this SNP in susceptibility to type 2 diabetes (Gaulton et al., 2008). Importantly, this association was replicated in an independent analysis (Burgdorf et al., 2011). These studies, combined with the finding that p53 plays a role in insulin resistance in mice (Minamino et al., 2009), prompted us to use a mouse model for the codon 72 polymorphic variants to shed light on the mechanism whereby these variants influence obesity, metabolism, and diabetic phenotypes. The mouse model uses a "humanized p53 knockin" (Hupki) of each variant that recapitulates human phenotypes (Frank et al., 2011; Luo et al., 2001). To study the association between the codon 72 polymorphism of p53 and diabetes, we studied the response of these mice to a high-fat diet (HFD).

RESULTS

R72 Hupki Mice Develop Excess Adiposity on a HFD

We analyzed isogenic P72 and R72 Hupki mice backcrossed to C57Bl/6J for over ten generations. Young male P72 and R72 mice between 4 and 6 weeks of age were fed a normal chow diet (CD) for 10 weeks, followed by a HFD for 8 weeks (see schematic; Figure 1A). Compared to P72 mice, R72 mice showed mildly increased weight gain on the CD ($p = 0.05$). Notably, however, R72 mice showed markedly increased weight gain on the HFD, compared to P72 ($p = 0.002$ at week 18; Figures 1B and 1C). The increased weight gain in HFD R72 mice was accompanied by an increased accumulation of fat in both subcutaneous and visceral areas (Figure 1D, red arrows). Body composition analysis with proton magnetic resonance spectroscopy (^{1}H-MRS) revealed that the body fat content was >20% greater in HFD R72 compared to P72 mice (Figures 1E and 1F). There was a modest increase in food consumption by R72 mice during the HFD period (Figures 1G and 1H), but analyses in metabolic cages revealed no differences in oxygen consumption, $C0_2$ release, food intake, physical activity, or other parameters in P72 and R72 mice that might have explained the increased weight gain (Figures S1A–S1G).

R72 Hupki Mice Develop More-Severe Glucose Intolerance and Insulin Resistance on a HFD

To determine whether the codon 72 polymorphism of p53 contributes to the development of phenotypes associated with type 2 diabetes, we performed glucose tolerance tests (GTTs) during the CD and HFD periods. After the CD, no differences in glucose tolerance were observed between P72 and R72 mice (Figures 2A and 2B). In contrast, after the HFD R72 mice showed significantly more-impaired glucose tolerance compared to P72 mice (Figures 2C, 2D, and S2A–S2D). Serum insulin levels were higher following fasting and glucose challenge in R72 compared to P72 mice (Figure 2E). This result suggested that R72-associated glucose intolerance is unlikely to be due to reduced insulin production. Upon examining the pancreas, we did not see significant differences in islet numbers, ratio of islet-associated endocrine cell populations, or proliferative potential of islet cells between P72 and R72 mice after HFD (Figures S2E–S2H). Interestingly, histopathological analysis of these pancreases revealed significantly larger islets in R72 mice (Figures 2F and 2G). R72 islets also showed increased levels of fibrosis, as assessed by Sirius Red staining; qRT-PCR analyses of genes associated with fibrosis confirmed this result (Figures 2H–2J). Moreover, R72 islets also showed increased senescence-associated β-galactosidase (SA-β-gal) (Figure S2I). The combined data suggest that, although R72 mice do not show evidence for impaired production of insulin after HFD, they do show signs of pancreatic dysfunction that are often seen in pre-diabetes. These results suggest that impaired glucose tolerance in R72 mice may be due to insulin resistance. To address this issue, a hyperinsulinemic-euglycemic clamp was performed to assess insulin sensitivity in R72 and P72 mice. The basal (fasting) blood glucose concentration and hepatic glucose production (HGP) were similar in R72 and P72 mice (Figures 2K and 2L). The glucose-infusion rate (GIR) needed to maintain euglycemia during the clamp was significantly lower in R72 than P72 mice, indicating insulin resistance (Figure 2M). There were non-significant reductions of the glucose disposal rate and HGP suppression during the insulin clamp in R72 compared to P72 mice, and the insulin-stimulated uptake of deoxyglucose trended lower in adipose and muscle tissues of R72 mice (Figures S2J–S2N), suggesting hepatic and peripheral insulin resistance in R72 mice following a HFD.

R72 Mice Develop Adipose Inflammation and NAFLD after HFD

The inflammatory response plays a critical role in the development of obesity and insulin resistance (Stienstra et al., 2011). p53 regulates insulin resistance in part through its ability to mediate an inflammatory response in adipose tissue (Minamino et al., 2009). Analysis of adipose tissue in P72 and R72 mice following a HFD revealed a markedly increased number of Adgre1 (F4/80)-positive monocytes/macrophages in the adipose tissue of R72 mice (Figures 3A, 3B, S3A, and S3B). R72 mice on a HFD developed markedly enlarged livers and signs of steatosis (Figures 3C–3E) and fibrosis (Figures 3F–3H). There was no increase in F4/80-positive cells in the R72 liver, but there was a dramatic increase in infiltrating cells staining positively for the phosphorylated form of the p65 subunit of NF-κB, indicative of increased inflammatory cells (Figures S3C–S3F). Elevated inflammation is a feature of non-alcoholic steatohepatitis (NASH) (Firneisz, 2014). NASH and non-alcoholic fatty liver disease (NAFLD) are closely associated with insulin resistance (Gruben et al., 2014). Moreover, p53 has been implicated in the progression from steatosis to NASH (Tomita et al., 2012). To demonstrate a connection between hepatic steatosis and insulin resistance in R72 mice, we examined the insulin-signaling pathway in the livers of the mice used for the hyperinsulinemic-euglycemic clamp experiments. The levels of p53 were similar in R72 and P72 livers following a HFD, but the phosphorylation of Akt1, a marker for insulin-signaling activity, was significantly decreased in the livers of R72 mice (Figures 3I and 3J). This demonstrates that hepatic insulin resistance is associated with steatosis and fibrosis in HFD R72 mice.

Altered Expression of p53-Regulated Genes in HFD R72 Liver

To explore the potential mechanisms underlying HFD-induced alterations in the liver, we performed qRT-PCR to evaluate the expression changes in the livers of HFD-fed mice of genes reported to be regulated by p53, particularly those with roles in the metabolism pathway (Goldstein and Rotter, 2012; Liang et al., 2013). Our initial analysis of known p53 target genes associated with cell-cycle arrest and apoptosis, including *Cdkn1a*(*p21*), *Mdm2*, *Pmaip1* (*Noxa*), and *Dram1* revealed no differences were observed in the expression of *Mdm2* and *Dram1* between P72 and R72 HFD livers. In contrast, the expression of *Cdkn1a*(*p21*) was increased 5-fold, and *Pmaip1* (*Noxa*) was increased 2-fold in the livers of R72 mice, compared to P72 (Figure 4A). It is of note that both *CDKN1A*(*p21*) and *PMAIP1* (*Noxa*) are biomarkers of NAFLD and NASH (Aravinthan et al., 2013; Bechmann et al., 2010).

These findings prompted us to analyze a larger set of p53-regulated genes in P72 and R72 livers following a HFD. In particular, we analyzed the expression of p53-regulated genes

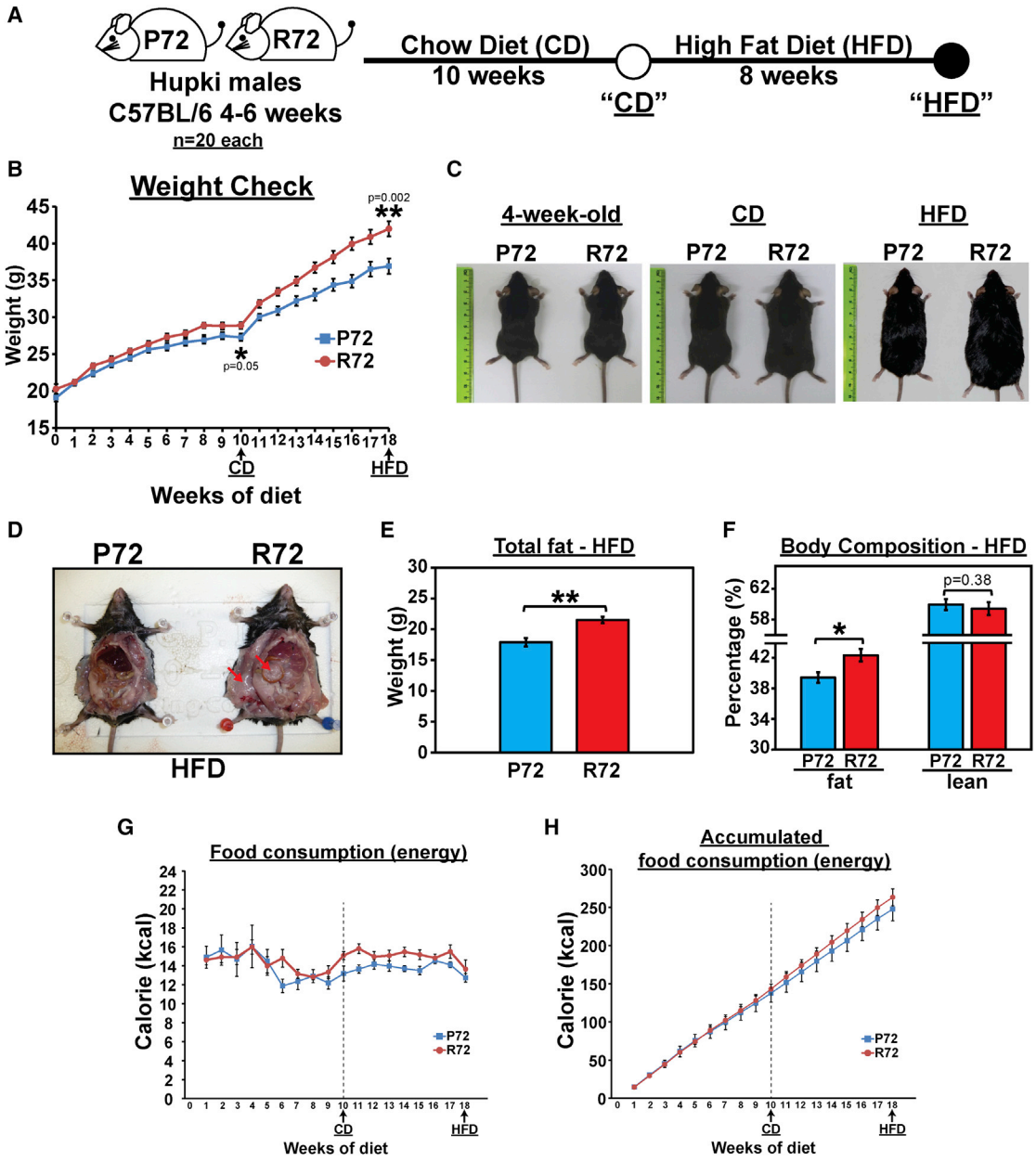

Figure 1. Higher Body Weight and Fat Content in R72 Hupki Mice on HFD

(A) P72 and R72 male mice of age 4–6 weeks (n = 20 each genotype) were fed a normal diet (chow diet [CD]) for 10 weeks and then switched to a high-fat diet (HFD) for 8 weeks. Mouse weight and food consumption were monitored weekly, and GTT was performed after both CD and HFD regimens.

(B) Progression of mouse weight throughout CD and HFD regimens; n = 20 each genotype. Error bars mark SE. The statistical trends of weight gain between P72 and R72 mice after CD and HFD were calculated using mixed effect models for longitudinal data analysis.

(C) Representative photos of P72 and R72 mice at the beginning of the experiment, post-CD, and post-HFD (left to right).

(D) Representative photos of P72 and R72 mice showing increased accumulation of subcutaneous and visceral fat in R72 mice. Arrows mark fat accumulation.

(E) Body fat mass measured by proton magnetic resonance spectroscopy (^{1}H-MRS) after HFD; n = 8 each genotype. Error bars mark SE. The double asterisk denotes $p < 0.005$.

(F) Body fat and lean mass measured by ^{1}H-MRS in HFD mice and normalized to whole body weight. The asterisk denotes $p < 0.05$.

(G) The average number of calories consumed by each mouse per week; n = 20 mice each genotype. Error bars mark SE. The dashed line marks the switch from CD to HFD after week 10.

(H) The accumulated number of calories consumed by each mouse throughout the study; n = 20 mice each genotype. Error bars mark SE. The dashed line marks the switch from CD to HFD after week 10.

See also Figure S1.

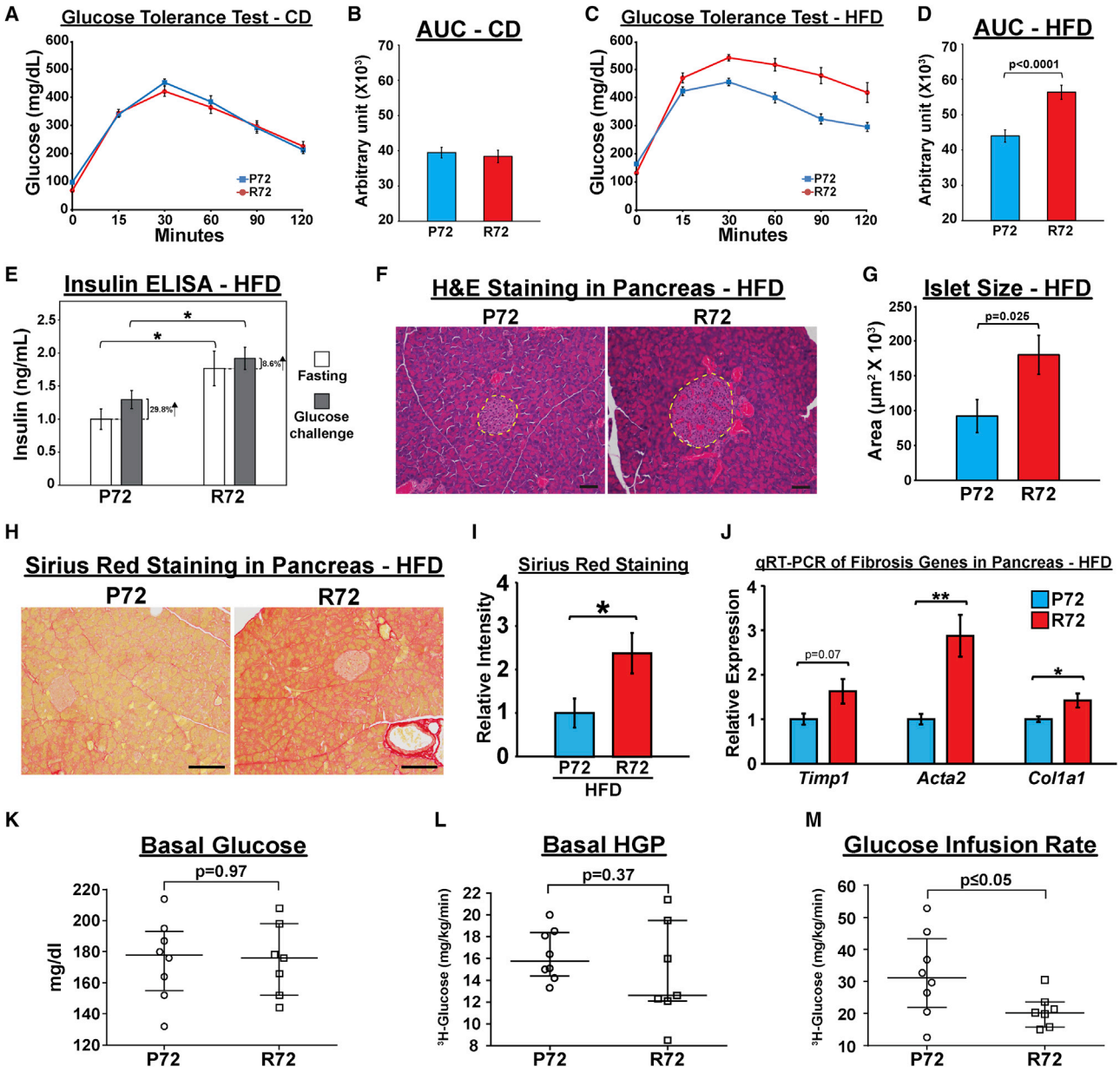

Figure 2. HFD Causes More-Severe Insulin Resistance in R72 Mice

(A) Glucose tolerance test (GTT) after CD. Mice were fasted for 16 hr and intraperitoneally injected with glucose solution (2 mg/g body weight). Blood glucose concentration was measured before the injection and at 15, 30, 60, 90, and 120 min post-injection; n = 20. Error bars are SEs.

(B) Quantification of AUC (area under curve) for GTT results after CD. Error bars mark SE.

(C) GTT after HFD; n = 20. Error bars mark SE.

(D) Quantification of AUC for GTT after HFD. Error bars mark SE.

(E) Serum insulin concentrations in mice before (fasting) and 15 min after intraperitoneal glucose injection (2 mg/g body weight); n = 10. Error bars are SEs. The asterisk denotes $p < 0.05$.

(F) H&E staining of the pancreas in HFD mice. Dashed lines mark pancreatic islets of Langerhans. The scale bar represents 50 μm.

(G) Average size of pancreatic islets in Hupki mice; n = 5. Error bars mark SE.

(H) Sirius Red staining to detect fibrosis in the pancreas after HFD. The scale bar represents 100 μm.

(I) Quantification of Sirius Red staining in pancreas between P72 and R72 mice after HFD; n = 5. Error bars mark SE. The asterisk denotes $p < 0.05$.

(J) qRT-PCR to detect mRNA levels of marker genes associated with fibrosis in pancreas after HFD; n = 4. Error bars mark SE. The single and double asterisks denote $p < 0.05$ and <0.005, respectively.

(K–M) Basal (6 hr fasting) blood glucose levels (K), hepatic glucose production (HGP) (L), and glucose infusion rate (M) during hyperinsulinemic-euglycemic clamp analysis in HFD mice; n = 8.

See also Figure S2.

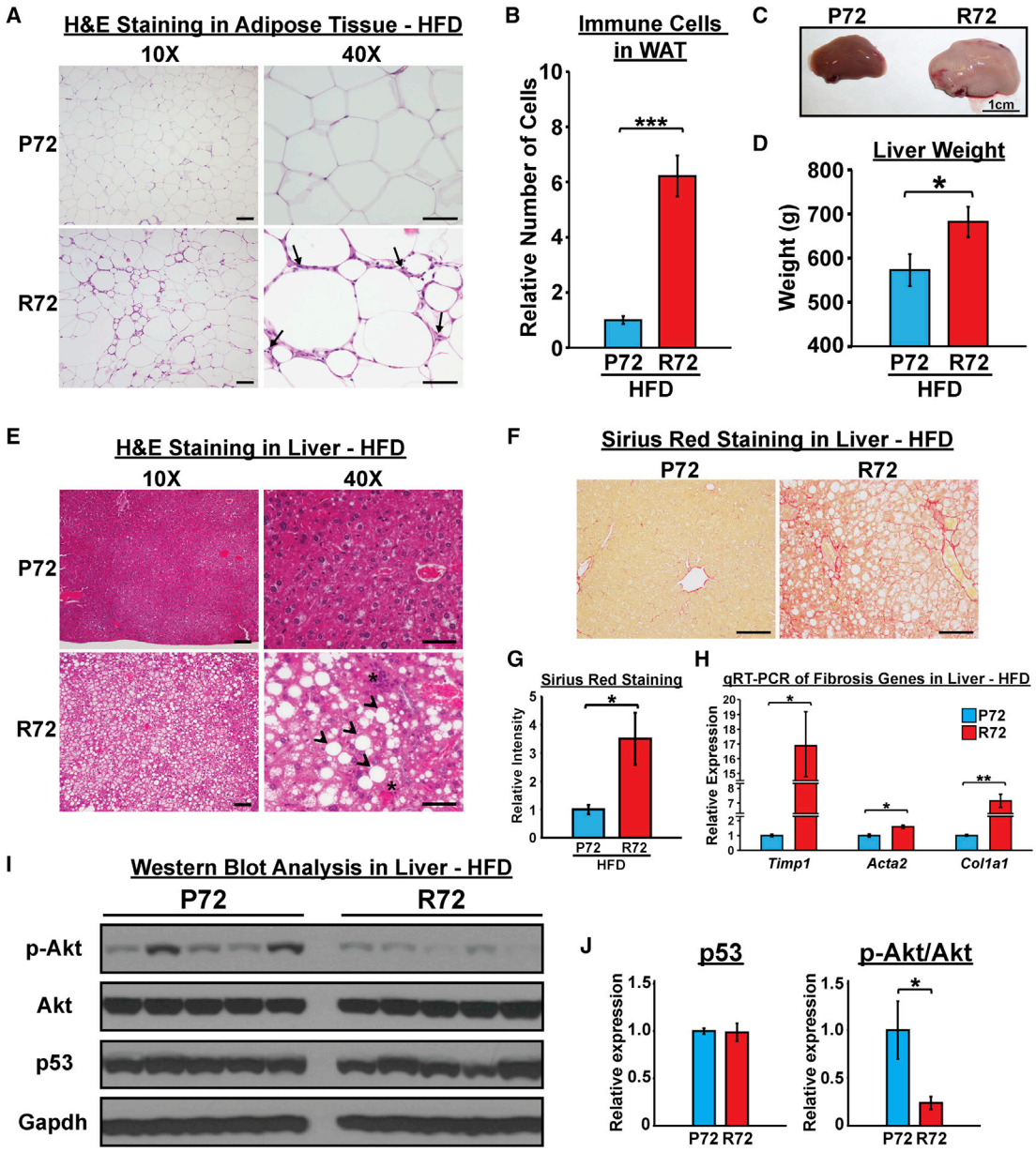

Figure 3. R72 Mice Develop More-Severe NAFLD after HFD

(A) Increased infiltration of immune cells in adipose tissues (arrows) in R72 mice, as shown by H&E staining post-HFD. The scale bar represents 100 μm in 10× and 50 μm in 40× images.

(B) Relative numbers of infiltrating immune cells in white adipose tissues between P72 and R72 mice; n = 5. Error bars mark SE. The triple asterisks denote $p < 0.0005$.

(C) Representative photos of livers post-HFD. The scale bar represents 1 cm.

(D) Average weight of left lateral lobe of livers between P72 and R72 mice after HFD; n = 8. Error bars mark SE. The asterisk denotes $p < 0.05$.

(E) H&E staining of livers post-HFD. Arrowheads mark formation of lipid droplets. Asterisks mark infiltrating immune cells. The scale bar represents 100 μm in 10× and 50 μm in 40× images.

(F) Sirius Red staining to detect fibrosis in liver after HFD. The scale bar represents 100 μm.

(G) Quantification of Sirius Red staining in liver between P72 and R72 mice after HFD; n = 5. Error bars mark SE. The asterisk denotes $p < 0.05$.

(H) qRT-PCR to detect mRNA levels of marker genes associated with fibrosis in liver after HFD; n = 4. Error bars mark SE. The single and double asterisks denote $p < 0.05$ and <0.005, respectively.

(I) Whole-cell lysates were extracted from livers of Hupki mice after hyperinsulinemic-euglycemic clamp analysis. Lysates were subjected to western blot analysis to detect p53, total Akt, and phosphorylated Akt at serine 473. Gapdh was used as the loading control.

(J) Quantification of signal intensities in (I) obtained using ImageJ software. The level of p53 was normalized to Gapdh, and the level of phosphorylated Akt (p-Akt) was normalized to the level of total Akt. Protein levels in P72 samples were set as 1-fold. Error bars mark SE. The asterisk denotes $p < 0.05$.

See also Figure S3.

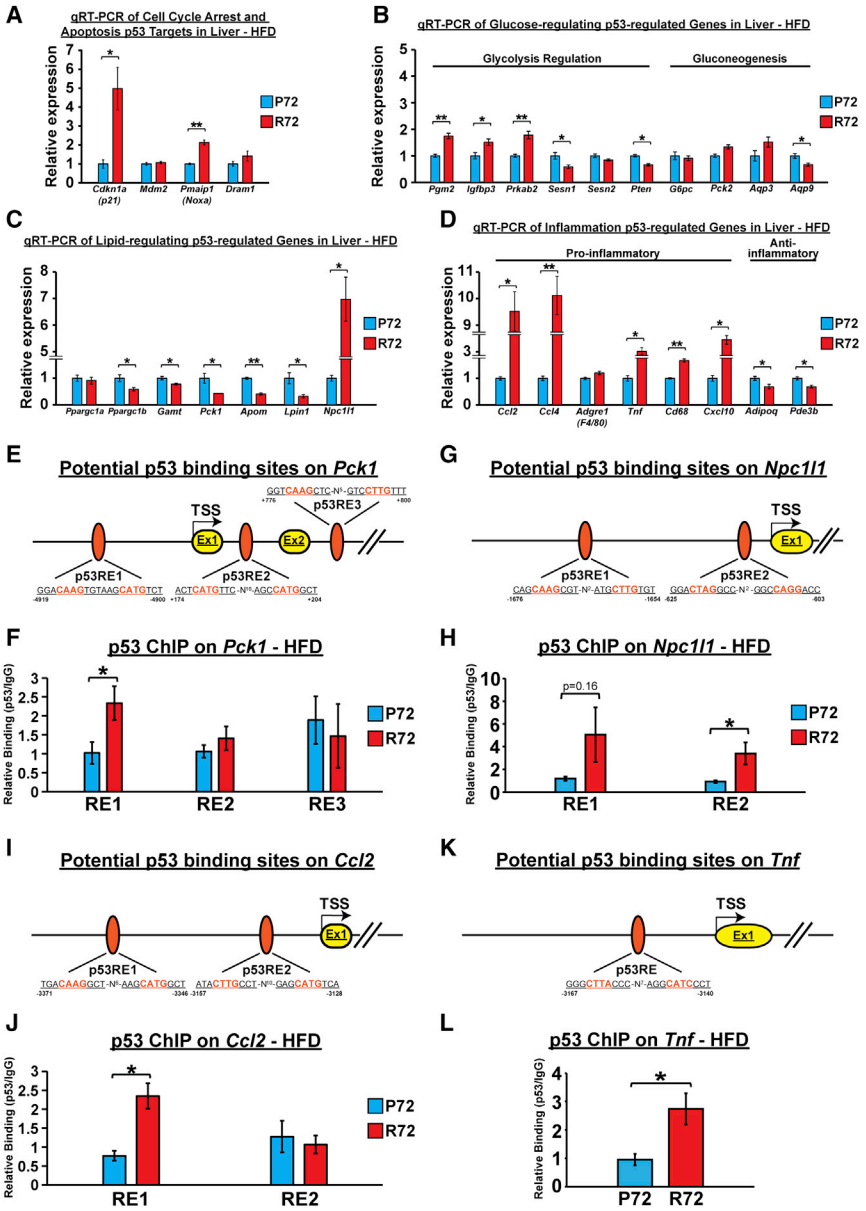

Figure 4. The Codon 72 Polymorphism of p53 Differentially Regulates DNA Binding and Expression of p53-Regulated Genes Associated with Lipid Metabolism and Inflammation

(A) qRT-PCR to detect mRNA levels of p53 target genes associated with cell-cycle arrest (*Cdkn1a*(*p21*) and *Mdm2*), senescence (*Cdkn1a*(*p21*)), and apoptosis (*Pmaip1*(*Noxa*) and *Dram1*) in livers of HFD-fed mice; n = 4. Error bars mark SE. The single and double asterisks denote $p < 0.05$ and <0.005, respectively.

(B) qRT-PCR to detect mRNA levels of p53-regulated genes associated with glucose homeostasis in livers of HFD-fed mice; n = 4. Error bars mark SE. The single and double asterisks denote $p < 0.05$ and <0.005, respectively.

(C) qRT-PCR to detect mRNA levels of p53-regulated genes associated with lipid metabolism in livers of HFD-fed mice; n = 4. Error bars mark SE. The single and double asterisks denote $p < 0.05$ and <0.005, respectively.

(D) qRT-PCR to detect mRNA levels of p53-regulated genes associated with inflammation in livers of HFD-fed mice; n = 4. Error bars mark SE. The single and double asterisks denote $p < 0.05$ and <0.005, respectively.

(E) Diagram of the *Pck1* gene, along with three potential p53 responsive elements (REs). The start site of transcription (TSS) is denoted +1, and the locations of potential p53 REs are shown relative to TSS. Ex, exon; N, spacers between consensus p53 half-sites.

(F) Chromatin immunoprecipitation of p53 in livers harvested from HFD-fed mice. Immunoprecipitated DNA was eluted and analyzed by qPCR using primers flanking potential *Pck1* p53 REs. Experiments were performed in triplicate from four biological replicates. Error bars mark SE. The asterisk denotes $p < 0.05$.

(G) Diagram of the *Npc1l1* gene, along with three potential p53 REs. The TSS is denoted +1, and the locations of potential p53 REs are shown relative to TSS.

(H) Chromatin immunoprecipitation of p53 in livers harvested from HFD-fed mice. Immunoprecipitated DNA was eluted and analyzed by qPCR using primers flanking potential *Npc1l1* p53 REs. Experiments were performed in triplicate from four biological replicates. Error bars mark SE. The asterisk denotes $p < 0.05$.

(I) Diagram of the *Ccl2* gene, along with three potential p53 REs. The TSS is denoted +1, and the locations of potential p53 REs are shown relative to TSS.

(J) Chromatin immunoprecipitation of p53 in livers harvested from HFD-fed mice. Immunoprecipitated DNA was eluted and analyzed by qPCR using primers flanking potential *Ccl2* p53 REs. Experiments were performed in triplicate from four biological replicates. Error bars mark SE. The asterisk denotes $p < 0.05$.

(K) Diagram of the *Tnf* gene, along with three potential p53 REs. The TSS is denoted +1, and the locations of potential p53 REs are shown relative to TSS.

(L) Chromatin immunoprecipitation of p53 in livers harvested from HFD-fed mice. Immunoprecipitated DNA was eluted and analyzed by qPCR using primers flanking potential *Tnf* p53 REs. Experiments were performed in triplicate from four biological replicates. Error bars mark SE. The asterisk denotes $p < 0.05$.

See also Figure S4.

associated with glycolysis (*Pgm2*, *Igfbp3*, *Prkab2*, *Sesn1*, *Sesn2*, and *Pten*), gluconeogenesis (*G6pc*, *Pck2*, *Aqp3*, and *Aqp9*), lipid metabolism (*Ppargc1a*, *Ppargc1b*, *Gamt*, *Pck1*, *Apom*, *Lpin1*, and *Npc1l1*), and inflammation (*Ccl2*, *Ccl4*, *Adgre1*(*F4/80*), *Tnf*, *Cd68*, *Cxcl10*, *Adipoq*, and *Pde3b*). Among the glycolysis- and gluconeogenesis-associated genes that we tested, there were no marked changes in gene expression, although three genes (*Pgm2*, *Igfbp3*, and *Prkab2*) showed modestly increased expression and three genes (*Sesn1*, *Pten*, and *Aqp9*) showed modestly reduced expression in R72 livers compared to P72 (Figure 4B). With regard to lipid-metabolism-associated genes, the R72 livers showed reduced expression of p53-regulated genes that positively regulate fatty acid oxidation (*Ppargc1b*, *Gamt*, and *Lpin1*) and lipid transport/elimination (*Pck1* and *Apom*). Notably,

Npc1l1, the main protein responsible for absorption of dietary cholesterol, was expressed 7-fold greater in R72 livers (Figure 4C). Additionally, there was a clear trend for an increased inflammatory signature in R72 livers. Several pro-inflammatory genes were significantly increased in R72 livers, whereas two anti-inflammatory genes (*Adipoq* and *Pde3b*) showed decreased expression (Figure 4D). Of these p53-regulated genes, four have been implicated in NAFLD and insulin resistance: *PCK1*, which is repressed by p53, and *TNF*, *CCL2*, and *NPC1L1*, which are induced by p53 (Hacke et al., 2010; Haukeland et al., 2006; Minamino et al., 2009; Nomura et al., 2009; She et al., 2000; Zhang et al., 2014). We confirmed the differences in protein level of Pck1, Ccl2, and Tnf by immunohistochemistry and western blotting (Figures S4A–S4J). We next performed chromatin immunoprecipitation to determine whether the R72 variant shows increased binding to the p53-response elements in these four genes. Notably, chromatin immunoprecipitation in the livers of HFD mice revealed increased binding of the R72 variant to at least one canonical p53-binding site in the promoters of all four genes, thus revealing increased DNA binding as the mechanism (Figures 4E–4L).

The Metabolic Phenotype in R72 Mice Is Exacerbated by a HFD

The possibility existed that R72 mice were prone to hepatic fat accumulation, steatosis, and fibrosis on a normal CD, as a result of aging or some other factor. Thus, we examined P72 and R72 male mice on a CD for 18 weeks (long CD or "LCD"). Similar to what we observed after 10 weeks of CD, R72 mice showed a mild increase in the body mass after LCD, along with a modest increase in body and liver fat accumulation (Figures 5A–5C and 5F–5I). Importantly, however, the GTT assay revealed no difference in glucose tolerance between P72 and R72 mice after LCD (Figures 5D and 5E). Additionally, there was no increase in Adgre1 (F4/80)-positive cells in the R72 adipose tissue compared to P72 (Figures S5A–S5C) and no evidence of increased inflammatory cells in R72 livers after LCD (Figures S5D–S5G). The gene expression profiles of p53-regulated genes revealed only two genes with modest increase in expression in R72 liver: *Ppargc1a* and *Cdkn1a*(*p21*) (Figures 5J–5L). These data indicate that the propensity for fat accumulation may be inherent to R72 mice but that the development of hepatic steatosis, fibrosis, and insulin resistance is greatly exacerbated by a HFD.

Tnf and *Npc1l1* Are "Early Responder" p53-Regulated Genes Induced following a HFD in R72 Livers

The physiological phenotypes associated with type 2 diabetes, such as obesity and inflammation, are known to form a positive feedback loop to exacerbate the disease (Ota, 2013). To gain a clearer picture of the sequence of events mediated by p53 following exposure to a HFD, we used a short-term (7-day) treatment with a HFD (short HFD or "SHFD") on 4-week-old male mice of both genotypes. Notably, after SHFD, R72 displayed significantly higher weight increase (Figures 6A–6C). We next analyzed in the livers of these mice the level of p53 and the expression of p53-regulated genes previously found to be differentially expressed between P72 and R72 after a long-term HFD. The steady-state level of p53 protein was similar between P72 and R72 before and after SHFD (Figures S6A and S6B), and we found no significant differences in the expression of any p53-regulated genes between P72 and R72, prior to exposure to SHFD (Figures S6C–S6E). After SHFD, three genes showed notable differences between P72 and R72 livers: these were *Npc1l1* (3-fold difference), *Cdkn1a*(*p21*) (2-fold difference), and *Tnf* (2-fold difference; Figures 6D–6F). Due to the differences in *Cdkn1a*(*p21*) on LCD shown previously, we chose to focus on *Npc1l1* and *Tnf* (Figure 5K). Immunohistochemical analysis of the livers of P72 and R72 mice showed no differences in control mice but markedly increased Tnf staining in R72 mice after SHFD (Figures 6G and 6I). This increase was accompanied by a marked accumulation of Tnf-positive cells in R72 adipose tissues (Figure S6F), a mild increase of hepatocyte vacuolization (Figure S6G), and increased fat accumulation in R72 livers, as assessed by Oil Red O staining (Figures 6H and 6J). These findings all preceded the signs of increased inflammation, as we detected no differences in the levels of inflammatory cells and macrophages present in the livers of P72 and R72 mice (Figures S6H and S6I). These results indicate that R72 mice appear to be more vulnerable to HFD-induced fat accumulation in the liver, even with limited exposure to a HFD. Further, these data suggest that genes such as *Tnf* and *Npc1l1* are "early responders" to a HFD in R72 livers and that these genes are likely involved with the initiation and subsequent development of NAFLD in R72 mice.

Increased *Tnf* and *Npc1l1* Underlie the R72 Response to a HFD

Because small-molecule inhibitors of Tnf and Npc1l1 were readily available, we sought to test whether these inhibitors could alleviate the effects of a short-term HFD (SHFD) in R72 mice. Toward this end, we treated both SHFD-fed P72 and R72 mice with daily treatment of C87, a Tnf inhibitor, or ezetimibe, an Npc1l1 inhibitor (Figure 7A). Both inhibitors led to significantly decreased percent weight gain and Oil Red staining (fat accumulation) in R72 mice compared to P72 mice, resulting in complete elimination of the increased fat accumulation (Figures 7B–7D) and weight gain (Figure S7) seen in R72 mice fed with a SHFD. These data firmly implicate these two p53-regulated genes in the differential response of R72 mice to a HFD.

DISCUSSION

In human studies, two groups found that the R72 variant of p53 is associated with increased risk for type 2 diabetes (Burgdorf et al., 2011; Gaulton et al., 2008). However, the underlying basis for this association was unknown. In this work, we took advantage of a mouse model of the codon 72 polymorphism of p53 to address this issue and found that mice possessing the R72 variant of p53 are more obesity prone and that this is associated with pathological changes in multiple tissues (Figure 7E). One of the strongest risk factors for type 2 diabetes is obesity (Wang et al., 2005). R72 Hupki mice gained weight more readily on either CD or HFD compared to P72 mice (Figure 1B). Moreover, the increased obesity phenotype in HFD R72 mice coincided with increased glucose intolerance and insulin resistance

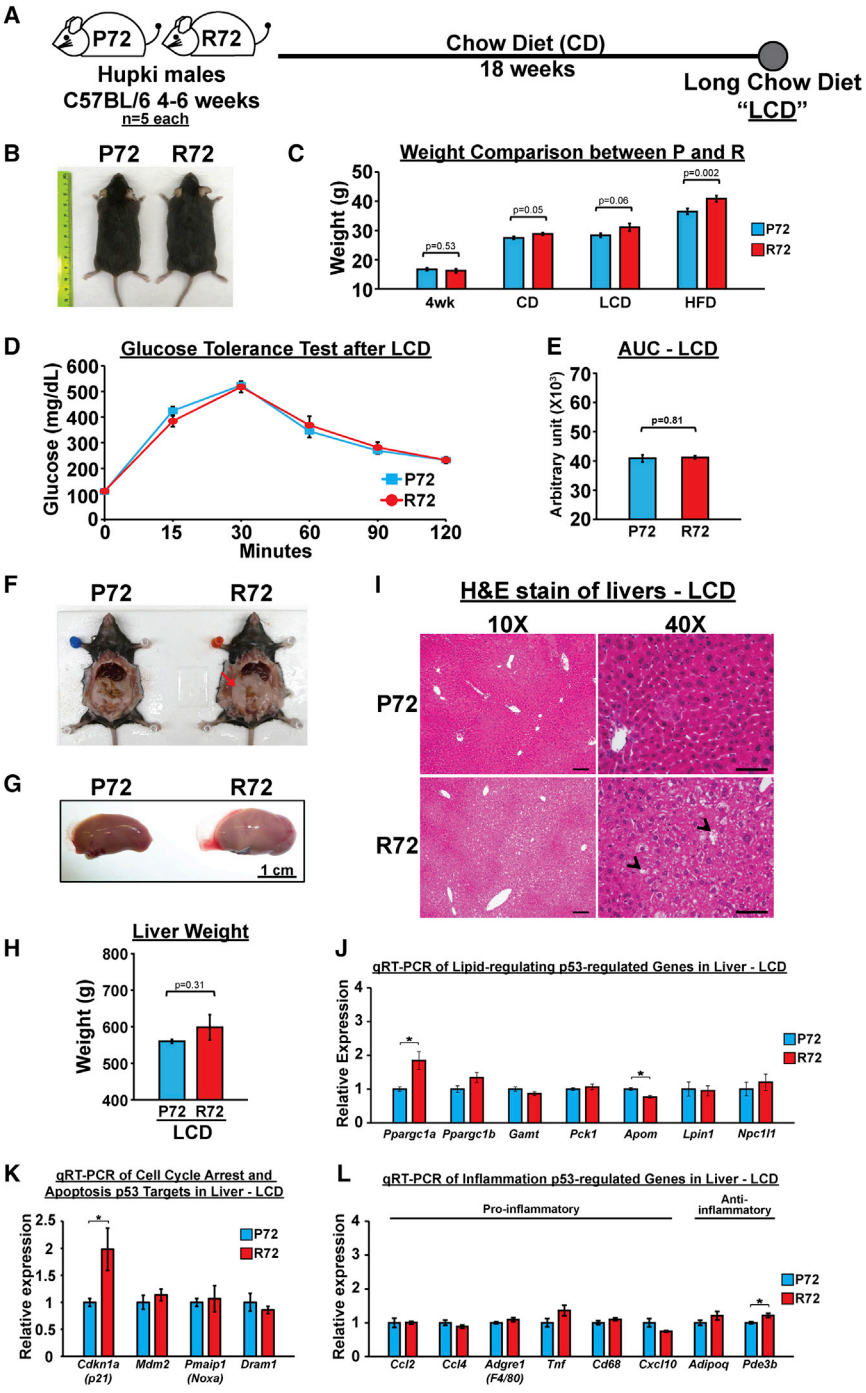

Figure 5. Increased Metabolic Dysfunction and Transcriptional Regulation in R72 Mice Are Dependent on a HFD

(A) P72 and R72 male mice of age 4–6 weeks (n = 5) were fed by CD for 18 weeks (long chow diet or "LCD").

(B) Representative images of P72 and R72 mice after LCD.

(C) Weight comparison between P72 and R72 mice at 4 weeks old or after different diet regimens.

(D) GTT after LCD; n = 20. Error bars mark SE.

(E) Quantification of AUC for GTT after LCD; n = 5. Error bars mark SE.

(F) Representative images of P72 and R72 mice showing slightly increased accumulation of visceral fat in R72 mice after LCD. The arrow marks fat accumulation.

(G) Representative images of livers after LCD. The scale bar represents 1 cm.

(H) Average weight of left lateral lobe of livers between P72 and R72 mice after LCD; n = 5. Error bars mark SE.

(I) H&E staining of livers after LCD. Arrowheads mark visible liver vacuolation. The scale bar represents 100 μm in 10× and 50 μm in 40× images.

(J–L) Total RNA were extracted from livers after LCD and subjected to qRT-PCR to detect mRNA levels of p53-regulated genes associated with (J) lipid metabolism, (K) cell-cycle arrest/senescence/apoptosis, and (L) inflammation; n = 3. Error bars mark SE. The asterisk denotes $p < 0.05$.

See also Figure S5.

(Figure 2). These data suggest that the R72 variant may predispose individuals to obesity, which subsequently leads to increased susceptibility to type 2 diabetes. In support of this hypothesis, a recent cohort study of over 2,500 Dutch and Finnish subjects found a significant association between R72 and increased waist circumference (Reiling et al., 2012). Similarly, a separate study showed that the association between BMI and diabetes is much stronger in homozygous R72 individuals (Gloria-Bottini et al., 2011). A recent study demonstrated that p53 protected against diet-induced obesity by inducing brown fat differentiation (Molchadsky et al., 2013). Therefore, one possibility based upon our combined findings and information in the literature is that instead of "promoting" obesity, the R72 variant may have impaired ability to suppress HFD-induced obesity. Our findings contradict a previous study using an exon 4 knockin mouse model for the codon 72 variants of p53. This study found no significant metabolic differences or pre-diabetic phenotypes in P72 and R72 mice (Reiling et al., 2014). However, the latter study did not use a HFD, only normal chow, and our data indicate that the phenotypes of P72 and R72 mice are very similar on normal chow. Instead, we find that a HFD effectively reveals the differences in metabolic phenotypes between P72 and R72 mice.

Evolutionarily, P72 first appears in the p53 gene of new world monkeys. Sequencing efforts have failed to detect the presence of R72 in other primates, suggesting that the emergence of modern human species coincided with the initial emergence of R72 (Puente et al., 2006). Whether this allele was subject to natural

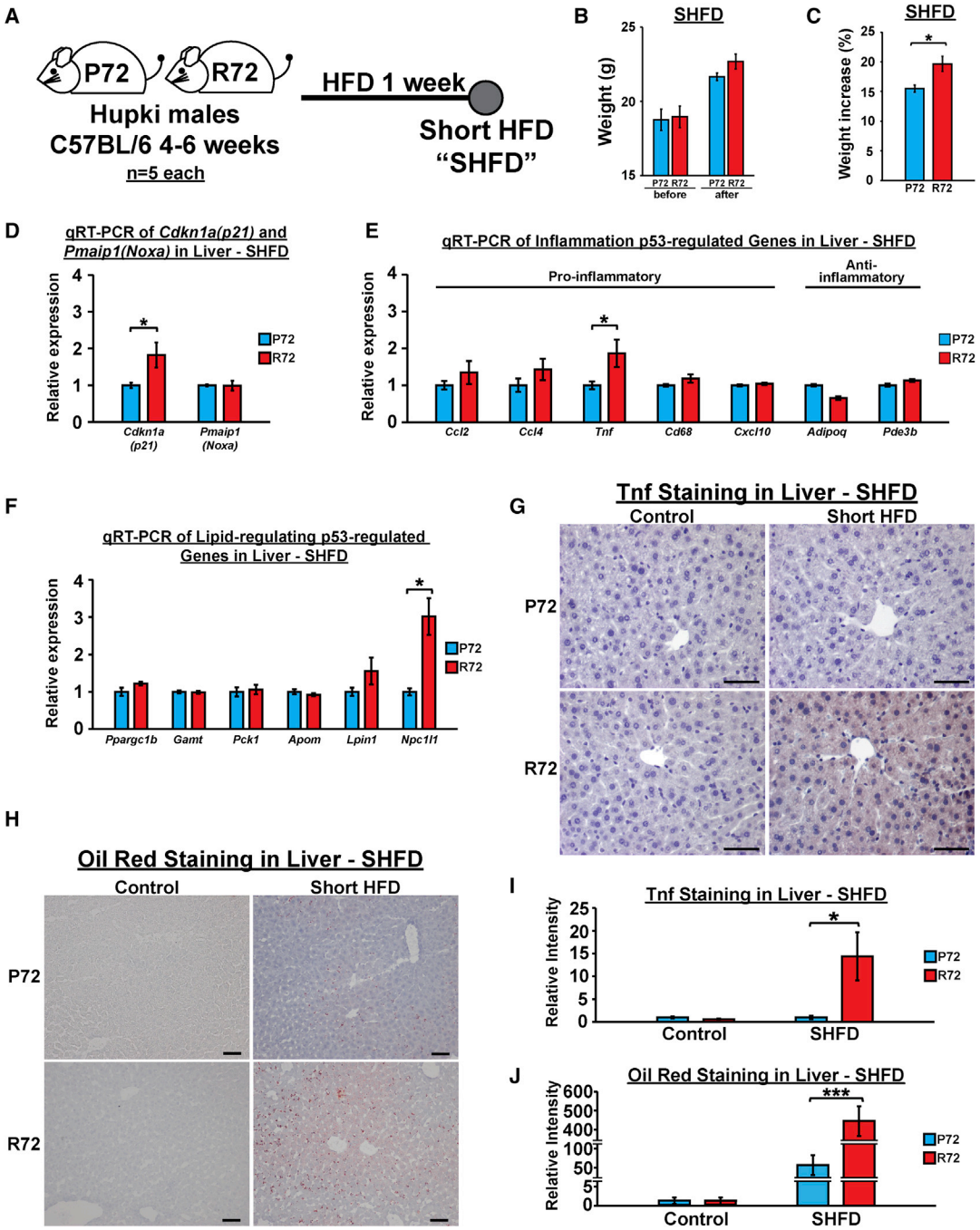

Figure 6. A Short-Term HFD in P72 and R72 Mice Reveals a Subset of "Early Responder" p53-Regulated Genes

(A) P72 and R72 male mice of age 4–6 weeks (n = 5) were fed by HFD for 1 week (short HFD or "SHFD").

(B) Average weight of Hupki mice before and after SHFD; n = 5.

(C) Average percent of weight increase of Hupki mice before and after SHFD; n = 5 mice each genotype. The asterisk denotes $p < 0.05$.

(D) mRNA levels of p53 target genes *Cdkn1a*(*p21*) and *Pmaip1*(*Noxa*) after SHFD; n = 4. Error bars mark SE. The asterisk denotes $p < 0.05$.

(E) mRNA levels of p53-regulated genes associated with lipid metabolism after SHFD; n = 4. Error bars mark SE. The asterisk denotes $p < 0.05$.

(F) mRNA levels of p53-regulated genes associated with inflammation after SHFD; n = 4. Error bars mark SE. The asterisk denotes $p < 0.05$.

(G) IHC staining of Tnf in Hupki mouse liver after SHFD. The scale bar represents 50 μm.

(H) Oil Red O staining of livers after SHFD. Red precipitation signals mark fat accumulation. The scale bar represents 100 μm.

(I) Quantification of Tnf staining in livers between P72 and R72 mice after SHFD; n = 5. Error bars mark SE. The asterisk denotes $p < 0.05$.

(J) Quantification of Oil Red staining in livers between P72 and R72 mice after SHFD; n = 5. Error bars mark SE. The triple asterisk denotes $p < 0.0005$.

See also Figure S6.

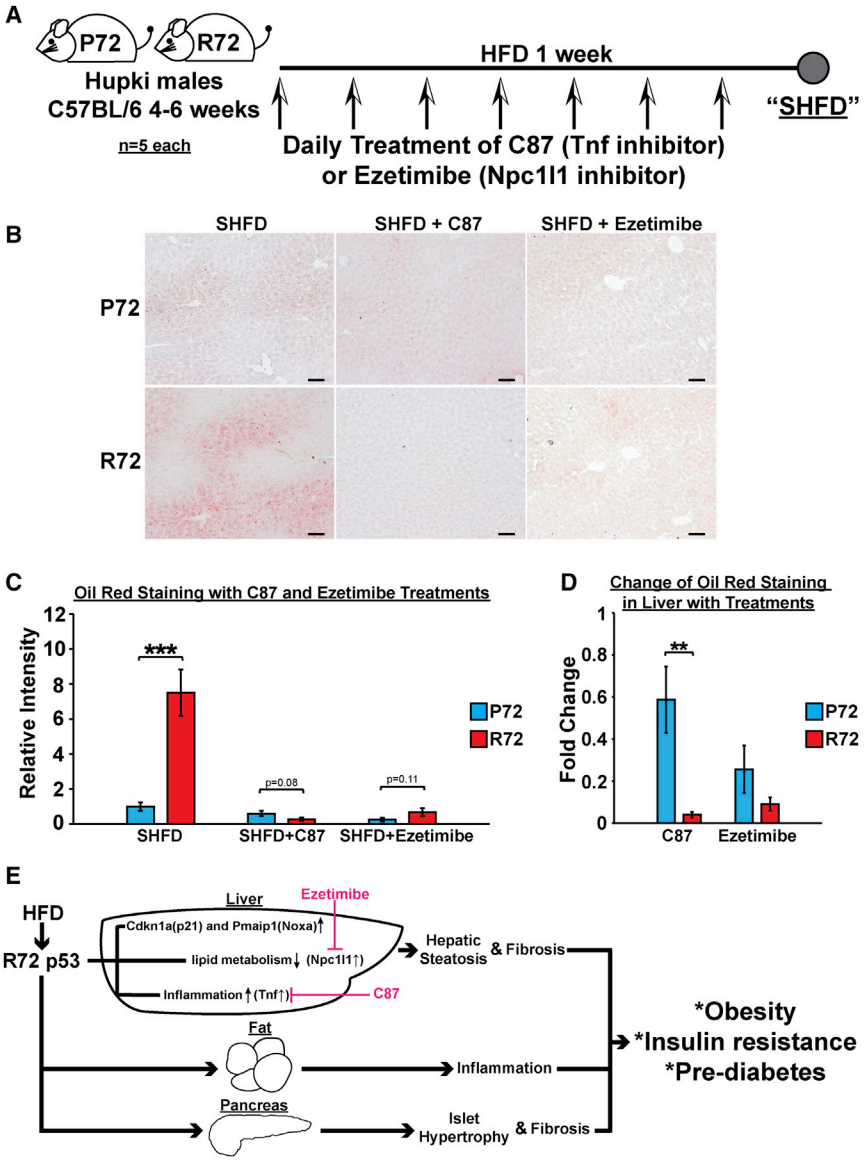

Figure 7. Tnf and Npc1l1 Inhibitions Rescue R72-Increased Fat Accumulation in the Liver after SHFD

(A) P72 and R72 male mice of age 4–6 weeks (n = 5) were subjected to SHFD with or without daily treatment of C87 (Tnf inhibitor) or ezetimibe (Npc1l1 inhibitor).

(B) Oil Red O staining of livers after SHFD with or without treatments of C87 or ezetimibe. The scale bar represents 100 μm.

(C) Quantification of Oil Red staining in livers between P72 and R72 mice after SHFD with or without treatments of C87 or ezetimibe; n = 5. Error bars mark SE. The triple asterisk denotes $p < 0.0005$.

(D) Average reduction of Oil Red staining in livers after SHFD with treatments of C87 or ezetimibe; n = 5. Error bars mark SE. The double asterisk denotes $p < 0.005$.

(E) Proposed model of the impact of R72 on obesity and pre-diabetic phenotypes. In R72 mice, a HFD results in obesity and insulin resistance. The effect of a HFD on R72 mice appears to be systematic, causing enlarged islets and fibrosis in the pancreas, increased infiltration of immune cells into adipose and liver tissues, as well as NAFLD. Inhibition of two R72-preferential p53-regulated genes, Tnf and Npc1l1, reduces fat accumulation in the liver. This could be a potential strategy to treat/prevent obesity and metabolic diseases associated with R72 genotype.

See also Figure S7.

selection remains controversial (Beckman et al., 1994; Khan et al., 2011; Sucheston et al., 2011). Multiple hypotheses have been posed in favor of natural selection, including that the R72 variant promotes optimal implantation and reproduction due to increased transactivation of the implantation factor LIF (Kang et al., 2009) or that it enhances tolerance to colder winter temperatures (Shi et al., 2009). In light of our experiments showing that R72 favors lipid accumulation and weight gain, we posit that R72 may have emerged during human evolution due to its ability to provide an advantage for environmental adaptations, such as famine and cold exposure. R72 would also be predicted to enhance the success of child-bearing during famine, which supports the fecundity hypothesis. We speculate that our ancestors may have undergone a positive selection for the R72 allele, which favored energy storage, as this would be advantageous during times of famine (Sellayah et al., 2014). However, in modern society, this positive selection is lost, and instead, the R72 allele is associated with obesity and type 2 diabetes. According to the most-recent genomic sequencing data, the R72 variant of p53 exists in approximately 5.6 billion people worldwide, of which 2.3 billion are homozygous (Abecasis et al., 2012). With a viable animal model, a better understanding of the mechanisms behind R72-associated obesity and diabetes has become feasible. Because obesity is also a risk factor for some forms of cancer, the association between R72 and obesity may explain the weak but persistent associations found between this codon 72 variant and cancer (Park et al., 2014).

Mechanistically, our work points to differences in at least two p53-regulated genes as potentially responsible for the obesity, insulin resistance, and NAFLD phenotypes evident in R72 mice. These genes, which show increased induction in the R72 liver at the earliest time points of HFD, but not CD, are *Tnf* and *Npc1l1*. Whereas our data clearly indicate that R72 protein binds preferentially to the p53-binding sites in these genes, we have failed to find evidence for differential phosphorylation or protein-protein interactions that may explain this differential binding ability (C.-P.K., unpublished data). Of these two genes, *Tnf* has been linked with obesity-induced insulin resistance, and recent studies show reduced blood glucose levels in patients treated

with TNF inhibitors (Antohe et al., 2012). *Npc1l1* plays a role in cholesterol absorption, and the Npc1l1 inhibitor ezetimibe lowers cholesterol levels and shifts HDL (high-density lipoprotein)-to-LDL (low-density lipoprotein) ratios (Park, 2013). Our data therefore clarify the potential association of the R72 variant of p53 with body waist circumference and type 2 diabetes. They also indicate that studies of the efficacy of some of these agents, such as TNF and NPC1L1 inhibitors, toward alleviating diabetes in humans may warrant further investigation.

EXPERIMENTAL PROCEDURES

Diet-Induced Obesity

The generation and analysis of Hupki P72 and R72 mice, and backcrossing in a C57Bl/6J background for over ten generations, was described previously (Frank et al., 2011). The experiments with mice complied with all federal and institutional guidelines as per IACUC protocols. Mice were housed in plastic cages with ad libitum diet and maintained at 22°C with a 12-hr dark/12-hr light cycle. Wild-type C57Bl/6 mice were purchased from The Jackson Laboratory. Normal CD was obtained from LabDiet (Pico-Vac Diet 20; 3.75 kcal/gm; 21% fat calories). The HFD was customized and purchased from Harlan Laboratories (TD. 130886; 4.4 kcal/g; 49% fat calories). Mouse weight and food consumption were monitored weekly throughout the duration of the experiments. Body composition (lean and fat mass) was measured with nuclear magnetic resonance spectroscopy (Echo MRI 3-in-1 analyzer). For rescue experiments with inhibitors, prior to 7-day exposure to a HFD, 5-week-old mice were weighed and then administered with tumor necrosis factor alpha (TNF-α) inhibitor C87 (10 mg/kg; EMD Millipore; 530796) or NPC1L1 inhibitor ezetimibe (10 mg/kg; Cayman Chemical; 16331) via intraperitoneal (i.p.) injection and oral gavage, respectively. Treatments were performed daily, and mice were weighed and euthanized for liver harvesting by the end of 7-day period.

GTT and Insulin ELISA

Mice were fasted overnight for 16 hr in cages with paper bedding. Each mouse was weighed, and glucose dose was calculated for 2 mg/kg body weight (glucose solution was prepared in 0.9% NaCl). Concentration of blood glucose of each mouse was determined by glucometer (OneTouch Ultra; LifeScan) in tail vein blood at time 0 before glucose was administered through i.p. injection. After injection, blood glucose level was measured at 15, 30, 45, 60, 90, and 120 min. For the insulin ELISA, mice were fasted overnight for 16 hr in cages with paper bedding. Glucose challenge was performed by i.p. injection at 2 mg/kg body weight. Blood was collected before the injection and at 10 min after the injection. Blood samples were kept at room temperature for 15 min and subject to centrifugation at 13,000 *g* for 10 min. Insulin concentration was measured in serum using an Ultra-Sensitive Mouse Insulin ELISA Kit (Crystal Chem; 90080).

Hyperinsulinemic-Euglycemic Clamp

Hyperinsulinemic-euglycemic clamp and radioisotopic tracer kinetic studies were done to evaluate insulin sensitivity in the whole body, as well as the liver, adipose tissue, and muscle as described previously (Carr et al., 2013). The mice were anesthetized, and the right internal jugular vein was cannulated. After 4 days of recovery to the pre-surgery weight, the mice were fasted for 6 hr (7 a.m.–1 p.m.) and a bolus intravenous injection of 5 μCi of [3-^{3}H] glucose was administered, followed by continuous intravenous infusion at 0.05 μCi/min. Baseline glucose kinetics was measured for 120 min followed by hyperinsulinemic clamping for 120 min. A priming dose of regular insulin (16 mU/kg; Humulin; Eli Lilly) was given intravenously, followed by a continuous infusion at 2.5 mU/kg/min. Blood glucose level was maintained at 140 mg/dl via a variable infusion of 20% glucose. 2-deoxy-D-[1-^{14}C] glucose was injected 45 min before the end of the clamping, and blood samples were collected to estimate glucose uptake. The mice were euthanized, and liver, epididymal white adipose tissue (WAT), and gastrocnemius muscle were excised, frozen immediately in liquid nitrogen, and stored at −80°C for analysis of glucose uptake.

Statistical Analysis

Data are expressed as means ± SEM. For statistical analysis, data were analyzed by two-sided unpaired Student's t test (GraphPad Prism), ANOVA post hoc test with Bonferroni's adjustment (for GTT AUC analysis), or mixed effect models for longitudinal data analysis (for the trends of weight gain between groups). Data were considered significant if $p < 0.05$.

SUPPLEMENTAL INFORMATION

Supplemental Information includes Supplemental Experimental Procedures and seven figures and can be found with this article online at http://dx.doi.org/10.1016/j.celrep.2016.02.037.

AUTHOR CONTRIBUTIONS

Conceptualization, C.-P.K., R.S.A., and M.E.M.; Methodology, C.-P.K., F.A.-D., D.L.G., R.S.A., and M.E.M.; Formal Analysis, C.-P.K. and Q.L.; Investigation, C.-P.K., J.I.-J.L., S.B., S.K., and F.A.-D.; Writing – Original Draft, C.-P.K. and M.E.M.; Writing – Review & Editing, C.-P.K., D.L.G., R.S.A., and M.E.M.; Funding Acquisition, R.S.A., D.L.G., and M.E.M.; Resources, J.I.-J.L., F.A.-D., D.L.G., R.S.A., and M.E.M.; Supervision, D.L.G., R.S.A., and M.E.M.

ACKNOWLEDGMENTS

We would like to thank Frederick Keeney and James Hayden for their assistance with imaging analysis, Dmitri Gourevitch for help with mouse tissue sectioning and H&E staining, and Marie Webster for help with senescence-associated β-galactosidase staining. We would like to thank Alex Kist and Abbey Goldenberg for blinded counting of IHC images as well as Matt Jennis and Jeremy Scott for their help with in vivo experiments. This project was supported by NIH grant CA102184 (to M.E.M.), P01 CA114046-07 (to D.L.G.), the Penn Diabetes Research Center Mouse Phenotyping Core grant P30DK19525, and the Penn Molecular Pathology & Imaging Core grant P30DK050306. Support for Core Facilities utilized in this study was provided by Cancer Center Support Grant (CCSG) CA010815 to The Wistar Institute.

Received: August 19, 2015
Revised: December 21, 2015
Accepted: February 3, 2016
Published: March 3, 2016

REFERENCES

Abecasis, G.R., Auton, A., Brooks, L.D., DePristo, M.A., Durbin, R.M., Handsaker, R.E., Kang, H.M., Marth, G.T., and McVean, G.A.; 1000 Genomes Project Consortium (2012). An integrated map of genetic variation from 1,092 human genomes. Nature *491*, 56–65.

Antohe, J.L., Bili, A., Sartorius, J.A., Kirchner, H.L., Morris, S.J., Dancea, S., and Wasko, M.C. (2012). Diabetes mellitus risk in rheumatoid arthritis: reduced incidence with anti-tumor necrosis factor α therapy. Arthritis Care Res. (Hoboken) *64*, 215–221.

Aravinthan, A., Scarpini, C., Tachtatzis, P., Verma, S., Penrhyn-Lowe, S., Harvey, R., Davies, S.E., Allison, M., Coleman, N., and Alexander, G. (2013). Hepatocyte senescence predicts progression in non-alcohol-related fatty liver disease. J. Hepatol. *58*, 549–556.

Azzam, G., Wang, X., Bell, D., and Murphy, M.E. (2013). CSF1 is a novel p53 target gene whose protein product functions in a feed-forward manner to suppress apoptosis and enhance p53-mediated growth arrest. PLoS ONE *8*, e74297.

Bechmann, L.P., Gieseler, R.K., Sowa, J.P., Kahraman, A., Erhard, J., Wedemeyer, I., Emons, B., Jochum, C., Feldkamp, T., Gerken, G., and Canbay, A. (2010). Apoptosis is associated with CD36/fatty acid translocase upregulation in non-alcoholic steatohepatitis. Liver Int. *30*, 850–859.

Beckman, G., Birgander, R., Själander, A., Saha, N., Holmberg, P.A., Kivelä, A., and Beckman, L. (1994). Is p53 polymorphism maintained by natural selection? Hum. Hered. *44*, 266–270.

Bergamaschi, D., Samuels, Y., Sullivan, A., Zvelebil, M., Breyssens, H., Bisso, A., Del Sal, G., Syed, N., Smith, P., Gasco, M., et al. (2006). iASPP preferentially binds p53 proline-rich region and modulates apoptotic function of codon 72-polymorphic p53. Nat. Genet. *38*, 1133–1141.

Burgdorf, K.S., Grarup, N., Justesen, J.M., Harder, M.N., Witte, D.R., Jørgensen, T., Sandbæk, A., Lauritzen, T., Madsbad, S., Hansen, T., and Pedersen, O.; DIAGRAM Consortium (2011). Studies of the association of Arg72Pro of tumor suppressor protein p53 with type 2 diabetes in a combined analysis of 55,521 Europeans. PLoS ONE *6*, e15813.

Carr, R.M., Dhir, R., Yin, X., Agarwal, B., and Ahima, R.S. (2013). Temporal effects of ethanol consumption on energy homeostasis, hepatic steatosis, and insulin sensitivity in mice. Alcohol. Clin. Exp. Res. *37*, 1091–1099.

Chang, J.R., Ghafouri, M., Mukerjee, R., Bagashev, A., Chabrashvili, T., and Sawaya, B.E. (2012). Role of p53 in neurodegenerative diseases. Neurodegener. Dis. *9*, 68–80.

Chen, Y., and Shen, Z. (2015). Gene polymorphisms in the folate metabolism and their association with MTX-related adverse events in the treatment of ALL. Tumour Biol. *36*, 4913–4921.

Danilova, N., Sakamoto, K.M., and Lin, S. (2008). p53 family in development. Mech. Dev. *125*, 919–931.

De Iuliis, F., Salerno, G., Taglieri, L., and Scarpa, S. (2015). Are pharmacogenomic biomarkers an effective tool to predict taxane toxicity and outcome in breast cancer patients? Literature review. Cancer Chemother. Pharmacol. *76*, 679–690.

Dumont, P., Leu, J.I., Della Pietra, A.C., 3rd, George, D.L., and Murphy, M. (2003). The codon 72 polymorphic variants of p53 have markedly different apoptotic potential. Nat. Genet. *33*, 357–365.

Firneisz, G. (2014). Non-alcoholic fatty liver disease and type 2 diabetes mellitus: the liver disease of our age? World J. Gastroenterol. *20*, 9072–9089.

Frank, A.K., Leu, J.I., Zhou, Y., Devarajan, K., Nedelko, T., Klein-Szanto, A., Hollstein, M., and Murphy, M.E. (2011). The codon 72 polymorphism of p53 regulates interaction with NF-kappaB and transactivation of genes involved in immunity and inflammation. Mol. Cell. Biol. *31*, 1201–1213.

Gaulton, K.J., Willer, C.J., Li, Y., Scott, L.J., Conneely, K.N., Jackson, A.U., Duren, W.L., Chines, P.S., Narisu, N., Bonnycastle, L.L., et al. (2008). Comprehensive association study of type 2 diabetes and related quantitative traits with 222 candidate genes. Diabetes *57*, 3136–3144.

Gloria-Bottini, F., Banci, M., Saccucci, P., Magrini, A., and Bottini, E. (2011). Is there a role of p53 codon 72 polymorphism in the susceptibility to type 2 diabetes in overweight subjects? A study in patients with cardiovascular diseases. Diabetes Res. Clin. Pract. *91*, e64–e67.

Goldstein, I., and Rotter, V. (2012). Regulation of lipid metabolism by p53 - fighting two villains with one sword. Trends Endocrinol. Metab. *23*, 567–575.

Gruben, N., Shiri-Sverdlov, R., Koonen, D.P., and Hofker, M.H. (2014). Nonalcoholic fatty liver disease: A main driver of insulin resistance or a dangerous liaison? Biochim. Biophys. Acta *1842*, 2329–2343.

Hacke, K., Rincon-Orozco, B., Buchwalter, G., Siehler, S.Y., Wasylyk, B., Wiesmüller, L., and Rösl, F. (2010). Regulation of MCP-1 chemokine transcription by p53. Mol. Cancer *9*, 82.

Haukeland, J.W., Damås, J.K., Konopski, Z., Løberg, E.M., Haaland, T., Goverud, I., Torjesen, P.A., Birkeland, K., Bjøro, K., and Aukrust, P. (2006). Systemic inflammation in nonalcoholic fatty liver disease is characterized by elevated levels of CCL2. J. Hepatol. *44*, 1167–1174.

Kang, H.J., Feng, Z., Sun, Y., Atwal, G., Murphy, M.E., Rebbeck, T.R., Rosenwaks, Z., Levine, A.J., and Hu, W. (2009). Single-nucleotide polymorphisms in the p53 pathway regulate fertility in humans. Proc. Natl. Acad. Sci. USA *106*, 9761–9766.

Khan, M.M., Rydén, A.M., Chowdhury, M.S., Hasan, M.A., and Kazi, J.U. (2011). Maximum likelihood analysis of mammalian p53 indicates the presence of positively selected sites and higher tumorigenic mutations in purifying sites. Gene *483*, 29–35.

Kung, C.P., Khaku, S., Jennis, M., Zhou, Y., and Murphy, M.E. (2015). Identification of TRIML2, a novel p53 target, that enhances p53 SUMOylation and regulates the transactivation of proapoptotic genes. Mol. Cancer Res. *13*, 250–262.

Levine, A.J., and Oren, M. (2009). The first 30 years of p53: growing ever more complex. Nat. Rev. Cancer *9*, 749–758.

Levine, A.J., Tomasini, R., McKeon, F.D., Mak, T.W., and Melino, G. (2011). The p53 family: guardians of maternal reproduction. Nat. Rev. Mol. Cell Biol. *12*, 259–265.

Li, T., Kon, N., Jiang, L., Tan, M., Ludwig, T., Zhao, Y., Baer, R., and Gu, W. (2012). Tumor suppression in the absence of p53-mediated cell-cycle arrest, apoptosis, and senescence. Cell *149*, 1269–1283.

Liang, Y., Liu, J., and Feng, Z. (2013). The regulation of cellular metabolism by tumor suppressor p53. Cell Biosci. *3*, 9.

Long, J.S., Crighton, D., O'Prey, J., Mackay, G., Zheng, L., Palmer, T.M., Gottlieb, E., and Ryan, K.M. (2013). Extracellular adenosine sensing-a metabolic cell death priming mechanism downstream of p53. Mol. Cell *50*, 394–406.

Luo, J.L., Yang, Q., Tong, W.M., Hergenhahn, M., Wang, Z.Q., and Hollstein, M. (2001). Knock-in mice with a chimeric human/murine p53 gene develop normally and show wild-type p53 responses to DNA damaging agents: a new biomedical research tool. Oncogene *20*, 320–328.

Maddocks, O.D., Berkers, C.R., Mason, S.M., Zheng, L., Blyth, K., Gottlieb, E., and Vousden, K.H. (2013). Serine starvation induces stress and p53-dependent metabolic remodelling in cancer cells. Nature *493*, 542–546.

Menendez, D., Shatz, M., and Resnick, M.A. (2013). Interactions between the tumor suppressor p53 and immune responses. Curr. Opin. Oncol. *25*, 85–92.

Minamino, T., Orimo, M., Shimizu, I., Kunieda, T., Yokoyama, M., Ito, T., Nojima, A., Nabetani, A., Oike, Y., Matsubara, H., et al. (2009). A crucial role for adipose tissue p53 in the regulation of insulin resistance. Nat. Med. *15*, 1082–1087.

Molchadsky, A., Ezra, O., Amendola, P.G., Krantz, D., Kogan-Sakin, I., Buganim, Y., Rivlin, N., Goldfinger, N., Folgiero, V., Falcioni, R., et al. (2013). p53 is required for brown adipogenic differentiation and has a protective role against diet-induced obesity. Cell Death Differ. *20*, 774–783.

Nomura, M., Ishii, H., Kawakami, A., and Yoshida, M. (2009). Inhibition of hepatic Niemann-Pick C1-like 1 improves hepatic insulin resistance. Am. J. Physiol. Endocrinol. Metab. *297*, E1030–E1038.

Ortega, F.J., Moreno-Navarrete, J.M., Mayas, D., Serino, M., Rodriguez-Hermosa, J.I., Ricart, W., Luche, E., Burcelin, R., Tinahones, F.J., Frühbeck, G., et al. (2014). Inflammation and insulin resistance exert dual effects on adipose tissue tumor protein 53 expression. Int. J. Obes. *38*, 737–745.

Ota, T. (2013). Chemokine systems link obesity to insulin resistance. Diabetes Metab. J. *37*, 165–172.

Park, S.W. (2013). Intestinal and hepatic niemann-pick c1-like 1. Diabetes Metab. J. *37*, 240–248.

Park, J., Morley, T.S., Kim, M., Clegg, D.J., and Scherer, P.E. (2014). Obesity and cancer–mechanisms underlying tumour progression and recurrence. Nat. Rev. Endocrinol. *10*, 455–465.

Pim, D., and Banks, L. (2004). p53 polymorphic variants at codon 72 exert different effects on cell cycle progression. Int. J. Cancer *108*, 196–199.

Poyurovsky, M.V., and Prives, C. (2010). P53 and aging: A fresh look at an old paradigm. Aging (Albany, N.Y.) *2*, 380–382.

Puente, X.S., Velasco, G., Gutiérrez-Fernández, A., Bertranpetit, J., King, M.C., and López-Otín, C. (2006). Comparative analysis of cancer genes in the human and chimpanzee genomes. BMC Genomics *7*, 15.

Reiling, E., Lyssenko, V., Boer, J.M., Imholz, S., Verschuren, W.M., Isomaa, B., Tuomi, T., Groop, L., and Dollé, M.E. (2012). Codon 72 polymorphism (rs1042522) of TP53 is associated with changes in diastolic blood pressure over time. Eur. J. Hum. Genet. *20*, 696–700.

Reiling, E., Speksnijder, E.N., Pronk, A.C., van den Berg, S.A., Neggers, S.J., Rietbroek, I., van Steeg, H., and Dollé, M.E. (2014). Human TP53 polymorphism (rs1042522) modelled in mouse does not affect glucose metabolism and body composition. Sci. Rep. *4*, 4091.

Sano, M., Minamino, T., Toko, H., Miyauchi, H., Orimo, M., Qin, Y., Akazawa, H., Tateno, K., Kayama, Y., Harada, M., et al. (2007). p53-induced inhibition of Hif-1 causes cardiac dysfunction during pressure overload. Nature *446*, 444–448.

Sellayah, D., Cagampang, F.R., and Cox, R.D. (2014). On the evolutionary origins of obesity: a new hypothesis. Endocrinology *155*, 1573–1588.

She, P., Shiota, M., Shelton, K.D., Chalkley, R., Postic, C., and Magnuson, M.A. (2000). Phosphoenolpyruvate carboxykinase is necessary for the integration of hepatic energy metabolism. Mol. Cell. Biol. *20*, 6508–6517.

Shi, H., Tan, S.J., Zhong, H., Hu, W., Levine, A., Xiao, C.J., Peng, Y., Qi, X.B., Shou, W.H., Ma, R.L., et al. (2009). Winter temperature and UV are tightly linked to genetic changes in the p53 tumor suppressor pathway in Eastern Asia. Am. J. Hum. Genet. *84*, 534–541.

Speliotes, E.K., Willer, C.J., Berndt, S.I., Monda, K.L., Thorleifsson, G., Jackson, A.U., Lango Allen, H., Lindgren, C.M., Luan, J., Mägi, R., et al.; MAGIC; Procardis Consortium (2010). Association analyses of 249,796 individuals reveal 18 new loci associated with body mass index. Nat. Genet. *42*, 937–948.

Stienstra, R., van Diepen, J.A., Tack, C.J., Zaki, M.H., van de Veerdonk, F.L., Perera, D., Neale, G.A., Hooiveld, G.J., Hijmans, A., Vroegrijk, I., et al. (2011). Inflammasome is a central player in the induction of obesity and insulin resistance. Proc. Natl. Acad. Sci. USA *108*, 15324–15329.

Sucheston, L., Witonsky, D.B., Hastings, D., Yildiz, O., Clark, V.J., Di Rienzo, A., and Onel, K. (2011). Natural selection and functional genetic variation in the p53 pathway. Hum. Mol. Genet. *20*, 1502–1508.

Tavana, O., Puebla-Osorio, N., Sang, M., and Zhu, C. (2010). Absence of p53-dependent apoptosis combined with nonhomologous end-joining deficiency leads to a severe diabetic phenotype in mice. Diabetes *59*, 135–142.

Thomas, M., Kalita, A., Labrecque, S., Pim, D., Banks, L., and Matlashewski, G. (1999). Two polymorphic variants of wild-type p53 differ biochemically and biologically. Mol. Cell. Biol. *19*, 1092–1100.

Tomita, K., Teratani, T., Suzuki, T., Oshikawa, T., Yokoyama, H., Shimamura, K., Nishiyama, K., Mataki, N., Irie, R., Minamino, T., et al. (2012). p53/p66Shc-mediated signaling contributes to the progression of non-alcoholic steatohepatitis in humans and mice. J. Hepatol. *57*, 837–843.

Vousden, K.H., and Ryan, K.M. (2009). p53 and metabolism. Nat. Rev. Cancer *9*, 691–700.

Wang, Y., Rimm, E.B., Stampfer, M.J., Willett, W.C., and Hu, F.B. (2005). Comparison of abdominal adiposity and overall obesity in predicting risk of type 2 diabetes among men. Am. J. Clin. Nutr. *81*, 555–563.

Whibley, C., Pharoah, P.D., and Hollstein, M. (2009). p53 polymorphisms: cancer implications. Nat. Rev. Cancer *9*, 95–107.

Zhang, P., Tu, B., Wang, H., Cao, Z., Tang, M., Zhang, C., Gu, B., Li, Z., Wang, L., Yang, Y., et al. (2014). Tumor suppressor p53 cooperates with SIRT6 to regulate gluconeogenesis by promoting FoxO1 nuclear exclusion. Proc. Natl. Acad. Sci. USA *111*, 10684–10689.